Simultaneous inhibition of Sirtuin 3 and cholesterol homeostasis targets acute myeloid leukemia stem cells by perturbing fatty acid β-oxidation and inducing lipotoxicity

Cristiana O'Brien,[1] Tianyi Ling,[1] Jacob M. Berman,[2] Rachel Culp-Hill,[3] Julie A. Reisz,[3] Vincent Rondeau,[2] Soheil Jahangiri,[1,2] Jonathan St-Germain,[2] Vinitha Macwan,[2] Audrey Astori,[2] Andy Zeng,[2] Jun Young Hong,[4] Meng Li,[5] Min Yang,[4] Sadhan Jana,[4] Fabia Gamboni,[3] Emily Tsao,[1] Weiyi Liu,[2] John E. Dick,[2] Hening Lin,[6] Ari Melnick,[5] Anastasia Tikhonova,[1,2] Andrea Arruda,[1] Mark D. Minden,[1,2] Brian Raught,[1,2] Angelo D'Alessandro[3] and Courtney L. Jones[1,2]

[1]Department of Medical Biophysics, University of Toronto, Toronto, Ontario, Canada; [2]Princess Margaret Cancer Center, University Health Network, Toronto, Ontario, Canada; [3]Biochemistry and Molecular Genetics, University of Colorado Anschutz Medical Campus, Aurora, CO, USA; [4]Department of Chemistry and Chemical Biology, Cornell University, Ithaca, NY, USA; [5]Department of Medicine, Division of Hematology & Medical Oncology, Weill Cornell Medical College, New York, NY, USA and [6]Howard Hughes Medical Institute; Department of Chemistry and Chemical Biology, Cornell University, Ithaca, NY, USA

Correspondence: C.L. Jones
Courtney.jones@uhnresearch.ca

Received: August 5, 2022.
Accepted: March 30, 2023.
Early view: April 6, 2023.

https://doi.org/10.3324/haematol.2022.281894

Supplementary Information

Title: Sirtuin 3 inhibition targets fatty acid oxidation in acute myeloid leukemia stem cells

Cristiana O'Brien, Tianyi Ling, Jacob M. Berman, Rachel Culp-Hill, Julie A. Reisz, Vincent Rondeau, Soheil Jahangiri, Jonathan St-Germain, Vinitha Macwan, Audrey Astori, Andy Zeng, Jun Young Hong, Meng Li, Min Yang, Sadhan Jana, Fabia Gamboni, Emily Tsao, Weiyi Liu, John E. Dick, Hening Lin, Ari Melnick, Anastasia Tikhonova, Andrea Arruda, Mark D. Minden, Brian Raught, Angelo D'Alessandro, Courtney L. Jones

Supplemental Methods:

Cell Culture

Molm13, MV4;11 cells were maintained in RPMI-1640 media with 10% fetal bovine serum (FBS). TEX[1] and OCI-AML-2 (obtained from Dr. Aaron Schimmer's Lab) cells were maintained in IMDM with 20% and 10% of FBS, respectively. IL-3 and SCF were added to TEX media. OCI-AML-3 were maintained in αMEM with 10% FBS. 293 T-REx cells were maintained in DMEM with 10% FBS. Cell lines were cultured with 100 units/mL penicillin and 100 µg/mL of streptomycin. Patient AML cells and healthy mobilized peripheral blood cells (MPBC) were obtained from the Princess Margaret Leukemia Tissue Bank and experiments were performed in accordance with UHN's Research Ethics Board, under protocol 20-5031. Human umbilical cord blood (CB) samples were obtained from Dr. John Dick's lab or purchased from stem cell technologies. CD34 enriched and whole bone marrow samples were purchased from Lonza.

Colony Forming Assays

Colony forming assays were performing using enriched (StemCell; 04435) or classic (StemCell; 04434) MethoCult media for primary AML or cell lines, respectively. Cells were treated for 24 hours with YC8-02 or transfected with siRNA using the methods described below. Colonies were counted 10-17 days after plating. Secondary replating of primary AML CFUs occurred 7-10 days after first plating. MethoCult containing colonies were washed and diluted with cell culture media. One fifth of each condition was replated into MethoCult media. Secondary CFUs were counted after 10-17 days.

Flow Cytometry

Viability was monitored using DAPI and AnnexinV-FITC (Biolegend; 640945) staining. For MPBC, cells were stained with DAPI, CD45-BB515 (BD564585), and CD34-PeCy7 (BD560710). Cells collected from engraftment studies were stained with CD45-BB515, CD34-BV421 (BD562577), CD38-PE-CF594 (BD562325), CD19-PE (BD555413), CD3-PECy7 (BD557749) and Live/Dead Far Red (Thermo Fisher; L34974). Addition of CD33-BV711 (BD563171) was used for normal bone marrow. All cells were sorted on Sony's SH800, MA900, or BD FACSAria Fusion and analysis was performed using the BD LSRFortessa and FlowJo. Cell number was determined

using CountBright Absolute Counting Beads (Thermo Fisher; C36950) or the integrated BD High-Throughput Sampler on the BD LSRFortessa.

Animal Studies

NSG-SGM3 mice 8-12 weeks of age were conditioned with busulfan (Sigma; B2635) at 25mg/kg IP (10% DMSO, 90% PBS), single injection 24 hours prior to engraftment. Primary cells (AML or healthy donor bone marrow) were plated as described previously and treated with YC8-02 (10uM) or vehicle 24 hours prior to engraftment. Alternatively, primary cells were transfected with siRNA targeting SIRT3 or a non-targeting scrambled control 24 hours prior to engraftment. Just before engraftment, cells were treated with OKT3 (BioXCell; BE0001-2) at 1ug/1 million cells in PBS, to deplete CD3+ immune cells and reduce the occurrence of graft-versus-host disease. Filtered, treated cells were injected via tail vein at a concentration of 1 million cells/ mouse. After engraftment was established (8-10 weeks), mice were sacrificed and both femurs were dissected out. The condyle was removed, and cells harvested via centrifugation. Cells were then treated with red blood cell lysis buffer (Sigma; 11814389001) to remove red blood cell fraction and evaluated by flow cytometry. CountBright absolute counting beads (Thermo Fisher; C36950) or an integrated High-Throughput Sampler was used to determine cell numbers.

Proximity-dependent biotin labeling (BioID)

SIRT3 complementary DNA was fused in-frame with a C-terminus BirA R118G – FLAG (BirA*FLAG) into a tetracycline-inducible pcDNA5 FLP recombinase target/tetracycline operator (FRT/TO) expression vector[2]. The Flp-In T-Rex 293 cells were then stably transfected with the SIRT3-BirA*FLAG or control (BirA*FLAG only). Cells were incubated with 1ug/mL tetracycline (Sigma-Aldrich) and 50uM biotin (BioShop) in complete DMEM supplemented with 10% FBS and 1% antibiotics for 24hr at 37°C with 5% CO2. Cells were scraped, washed once in PBS and lysed in RIPA buffer. The lysates were sonicated twice for 10 sec at 35% amplitude (Sonic Dismembrator 500; Fischer Scientific) and centrifuged at 16,000rpm for 30min at 4°C. Supernatants were then passed through Micro Bio-Spin Chromatography column (Bio-Rad) and incubated with high-performance streptavidin packed beads (GE Healthcare) for 3 hours at 4°C on an end-over-end rotator. Beads were collected and washed 6 times with 50mM ammonium bicarbonate and then treated with TPCK-trypsin (Promega) for 16 hours at 37°C on an end-over- end rotator.

The beads were further subjected to TPCK-trypsin (1uL) and incubated for 2 hours at 37°C on an end-over-end rotator. Supernatants were lyophilized for downstream MS analysis.

Lyophilized samples reconstituted in 0.1% HCOOH were loaded on a pre-column (C18 Acclaim PepMap^{TM} 100, 75uM x 2cm, 3um, 100Å) prior to chromatographic separation through an analytical column (C18 Acclaim PepMap^{TM} RSLC, 75um x 50cm, 3um, 100Å) by HPLC over a reversed-phase gradient (120-minute gradient, 5-30% CH3CN in 0.1% HCOOH) at 225nL/min on an EASY-nLC1200 pump in-line with a Q-Exactive HF mass spectrometer operated in positive ESI mode. An MS1 ion scan was performed performed at 60,000 fwhm followed by MS/MS scans (HCD, 15,000 fwhm) of the 20 most intense parent ions (minimum ion count of 1000 for activation). Dynamic exclusion (10 ppm) was set at 5 seconds.

To identify peptides and proteins, the raw files (.raw) containing information of the spectra of peptides was converted to .mzML format by Proteowizard (v3.0.19311). Then the spectras was searched by X!Tandem (v2013.06.15.1) and Comet (v2014.02.rev.2) against human RefSeqV104 database (containing 36,113 entries) to match and assign peptide sequence. Search parameters specified a parent ion mass tolerance of 15ppm and an MS/MS fragment ion tolerance of 0.4Da, with up to two missed cleavages allowed for trypsin. No fixed modifications was set. Deamidation (NQ), oxidation (M), acetylation (protein N-term), and diglycine (K) was set as variable modifications. Data was processed through the trans-proteomic pipeline (TPP v4.7).

Proteins were identified with an iProphet cut-off of 0.9 (corresponding to ≤1% FDR) and at least two unique peptides. High-confidence interactors were defined as those with a Bayesian false discovery rate (BFDR) of ≤0.01 following Significance Analysis of Interactome (SAINT). SIRT3 interactors were plotted with Cytoscape (v3.9.0).

SIRT3 Network analysis

Unique differentially expressed genes (DEGs) from LSCs or blasts post YC8-02 treatment were identified from RNA sequencing analysis (DEseq2) with adjusted p-values<0.05 (Benjamin-Hochberg adjustment). As BioID identified SIRT3 interactors are not cell type specific, DEGs identified through YC8-02 treatment in LSCs and blasts were used to refine the SIRT3 interactome based on cellular context. DEGs were cross-referenced to BioID identified SIRT3 interactors to create a SIRT3 LSC network or SIRT3 blast network (Supplemental table 3). Specifically, 45 BioID identified SIRT3 interactors which were differentially expressed in YC8-02-treated LSCs comprised an LSC-specific SIRT3 interaction network (SIRT3 LSC network),

while 9 BioID identified SIRT3 interactors which were differentially expressed in YC8-02-treated comprised a Blast-specific SIRT3 interaction network (SIRT3 Blast network). Enrichment for respective SIRT3 networks within LSCs and blast populations was scored using GSVA[3] on the following datasets: quantile-normalized RNA-sequencing data from sorted AML fractions[4]; TPM-normalized RNA-seq data collected from sorted AML fractions[5]; paired AML samples collected at diagnosis and relapse[6-9]; and diagnostic AML samples from three patient cohorts[10-12].

Enrichment of SIRT3 LSC and SIRT3 blast network genes was also compared against SIRT3 gene expression in LSCs and non-LSCs represented through quantile normalized values for microarray data, log(TPM+1) normalized values for RNA-seq data from diagnosis and relapse pairs, and vst normalized values for RNA-seq data from AML fractions and AML patient cohorts. For correlation analysis with other biological processes, GSVA was performed on 812 diagnostic AML samples using GO Biological Process gene sets from the MSigDB database and compared against SIRT3 Network enrichment scores.

Transfection of siRNA:

Cell lines and primary specimens were transfected with small interfering RNA (siRNA) constructs targeting SIRT3, or non-targeting scrambled siRNA (Horizon Discovery). Invitrogen Neon electroporator as previously described[13,14], using buffer T for primary cells and buffer R for cell lines at 1600V, 20ms, 3 pulses.

Metabolomics

For steady state metabolomics, primary AML and cell lines were collected post YC8-02 treatment, in triplicate, containing 1-2.5 x10^5 cells in 1.7mL microtubes. Each replicate was washed three times on ice with PBS. All buffer was aspirated from the cell pellet and flash frozen in liquid nitrogen vapors, prior to storage at -80°C. Metabolomic analyses were performed by mass spectrometry.

Thawed samples were resuspended in chilled extraction solution (methanol:acetonitrile:water (5:3:2 v/v)) at 2×10^6cells per mL of extraction solution. After vortexing for 30 min at 4°C, samples were centrifuged at 12,000 g for 10 min at 4°C and supernatants isolated for metabolomics analyses. . 10 µL of sample extract was run through a Kinetex C18 1.7 µm, 100 × 2.1 mm (Phenomenex) reversed phase column (Positive ion mode—phase A: water, 0.1% formic acid; B: acetonitrile, 0.1% formic acid; Negative ion mode—phase A: 1 mM NH4Ac 95:5 water:

acetonitrile; phase B: 1 mM NH4Ac 95:5 acetonitrile: water) via an ultra-high performance chromatographic system (UHPLC—Vanquish, Thermo Fisher). UHPLC was coupled in line with a high-resolution quadrupole Orbitrap instrument run in both polarity modes (QExactive, Thermo Fisher) at 70,000 resolution (at 200 m/z) and metabolites were separated through a 5 min gradient with the phases described above and the mass spectrometer operated either in positive or negative ion mode in separate runs. To quantify metabolite peaks, the raw files (.raw) containing information of the spectra of metabolites were converted to .mzXML using RawConverter. Metabolites were then assigned names using KEGG database by Maven software. The ratio of the peak areas for stable isotope labeled standards and unlabeled controls were used to determine the metabolite quantity in the extract.

Lipidomics

For steady state lipidomics, primary AML and cell lines were collected post YC8-02 treatment, in 4 replicates, containing 1-2.5 x10^5 cells in 1.7mL microtubes. Each replicate was washed three times on ice with PBS. All buffer was aspirated from the cell pellet and flash frozen in liquid nitrogen vapors, prior to storage at -80°C. Lipidomics analyses were performed by mass spectrometry.

Thawed samples were resuspended in chilled extraction solution (Methanol 50%) at 2×10^6cells per mL of extraction solution. Samples were incubated in the freezer at -20°C for 15 minutes prior to centrifugation and isolation of the supernatant for mass spectrometry. 10 µL of sample extract was run through a Kinetex C18 1.7 µm, 100 × 2.1 mm (Phenomenex) reversed phase column (Negative ion mode—phase A: 1 mM NH4Ac 95:5 water: acetonitrile; phase B: 1 mM NH4Ac 95:5 acetonitrile: water) via an ultra-high performance chromatographic system (UHPLC—Vanquish, Thermo Fisher). UHPLC was coupled in line with a high-resolution quadrupole Orbitrap instrument run in negative polarity mode (QExactive, Thermo Fisher) at 70,000 resolution (at 200 m/z) and metabolites were separated through a 5 min gradient with the phases described above and the mass spectrometer operated in negative ion mode. To quantify metabolite peaks, the raw files (.raw) containing information of the spectra of metabolites were converted to. mzXML using RawConverter. Metabolites were then assigned names using KEGG database by Maven software. The ratio of the peak areas for stable isotope labeled standards and unlabeled controls were used to determine the metabolite quantity in the extract.

Metabolic Flux

For palmitic flux metabolomics, primary AML and cell lines were treated with YC8-02 10μM for 4 hours in 4 replicates, containing 1-2.5 $x10^5$ cells in 1.7mL microtubes. Cells were introduced to either 16C13 Palmitate (Sigma; 605573) or 1C13 Palmitate (Sigma; 605646) at 100 μM final concentration. A subset was left unlabeled with heavy palmitate as biological control. Cells were collected after an additional 4 or 16 hours of incubation with palmitate. Each replicate was washed three times on ice with PBS. All buffer was aspirated from the cell pellet and flash frozen in liquid nitrogen vapors, prior to storage at -80°C.Cells were collected, and palmitate metabolism was assessed by mass spectrometry.

Thawed samples were resuspended in chilled extraction solution (Methanol 50%, acetonitrile 30%, and water 20% v/v) at $2×10^6$ cells per mL of extraction solution. After vortexing for 30 min at 4°C, samples were centrifuged at 12,000 g for 10 min at 4°C and supernatants isolated for metabolomics analyses. An ultra-high-pressure liquid chromatography system was used for chromatographic separation using an analytical column, Kinetex 1.7μm C18 100Å, UHPLC column 150×2.1mm (Phenomenex; 00F-4475-AN) with a guard column, SecurityGuard™ ULTRA cartridge-UHPLC C18 for 2.1mm ID columns (Phenomenex; AJ08782). 10uL of sample extract was injected onto the column. (Positive ion mode—phase A: water, 0.1% formic acid; B: acetonitrile, 0.1% formic acid; Negative ion mode—phase A: 1 mM NH4Ac 95:5 water: acetonitrile; phase B: 1 mM NH4Ac 95:5 acetonitrile: water) via an ultra-high performance chromatographic system (UHPLC—Vanquish, Thermo Fisher). UHPLC was coupled in line with a high-resolution quadrupole Orbitrap instrument run in both polarity modes (QExactive, Thermo Fisher) at 70,000 resolution (at 200 m/z) and metabolites were separated through a 5 min gradient with the phases described above and the mass spectrometer operated either in positive or negative ion mode in separate runs. To quantify metabolite peaks, the raw files (.raw) containing information of the spectra of metabolites were converted to .mzXML using RawConverter. Metabolites were then assigned names using KEGG database by Maven software. The ratio of the peak areas for stable isotope labeled standards and unlabeled controls were used to determine the metabolite quantity in the extract.

Seahorse

Metabolic analysis was conducted using Agilent's Seahorse XFe96 analyzer and the Mito Stress Test. Using Agilent's FluxPak (102416-100) the microplate was treated with Cell-Tak (Corning;

324240) prior to seeding 5 wells per condition with 1-2 × 10^5 of our cells of interest in Agilent's DMEM supplemented with glucose, pyruvate, and glutamine (103680-100). Sensor cartridges were incubated overnight using Calibrant solution at 37°C and prepared with Oligomycin [6.3µM] (Sigma-Aldrich; 871744), FCCP [2µM] (Sigma-Aldrich; C2920), Rotenone (Sigma-Aldrich; R8875)/Antimycin (Sigma-Aldrich; A8774) [5µM/5µM].

RNA Sequencing Analysis

Short read quality control was performed using *FastQC v0.11.5* (https://www.bioinformatics.babraham.ac.uk/projects/fastqc/). The sequencing adapters and low-quality end reads were trimmed using *Trim Galore v0.6.6* (https://www.bioinformatics.babraham.ac.uk/projects/trim_galore/). *STAR v.2.7.9a*[15] was used to align the raw reads to GENCODE human reference genome *v38*[16]. After removing low quality alignments, (*mapq* < 15), *featureCounts v2.0.1*[17] was used for gene expression quantification. After removing genes with less than 10 counts across all samples, *DESeq2 v1.32.0*[18] was used to identify differentially expressed genes between treatment and control groups, considering the primary sample batch in the model. Gene set enrichment analysis (GSEA)[19] was performed using *fgsea v1.18.0*[20] and Bader lab gene sets, updated August 2021 (http://baderlab.org/GeneSets)[21]. *Limma v3.48.3*[22] was used for gene expression batch correction. All p-values were adjusted using the Benjamin-Hochberg method[23].

Supplemental Tables:

Supplemental Table 1: Patient Characteristics

Code	Sample Source	Status	Age at Diagnosis	Sex	Diagnosis	FAB Classification	Cytogenetics	Mutated Genes
AML1	PB	Relapse	79	Male	AML		46,XY,t(6;9) (p21;q34)	FLT3 ITD, FLT3 TKD, IDH2
AML2	PB	Relapse	69	Female	AML		46,XX,add(14)(q22)[4]	FLT3, IDH1, NPM1
AML3	PB	Refractory	47	Male	AML		46,XY,del(7)(q21)[8]/46,sl,del(5)(q31q35),add(12)(p13)[7]/46,sl,add(12)(p13),del(17)(q21)[3]/46,XY,del(9)(q22q32)[2]	IDH1 Arg132; CKIT D816V
AML4	PB	Relapse	49	Female	AML		46,XX[21]	FLT3 ITD+
AML5	PB	Diagnosis	49	Female	AML		Normal Karyotype (46,XX)	FLT3-IDT+, WT for CEBPA, NPM1, IDH1, IDH2, and JAK2
AML6	PB	Diagnosis	87	Male	AML		46,XY[20]	WT for NPM1 and FLT3
AML7	PB	Diagnosis	77	Female	AML	M5a	46,XX,del(5)(q13q31)[6]/47,idem,+11[14]	DNMT3A Arg326Cys, FLT3-ITD, IDH2 Arg140Gln, KRAS Thr58Ile, TP53 Cys275Arg, NPM1 Mutant
AML8	PB	Diagnosis	82	Female	AML, NOS	M4	46,XX[20]	N/A
AML9	PB	Diagnosis	70	Female	AML, NOS	M1	46,XX[20]	N/A
AML10	PB	Diagnosis	94	Female	AML with t(8;21)(q22;q22)	M2	46,XX,t(8;21)(q22;q22)[8]	N/A
AML11	PB	Diagnosis	77	Male	AML, NOS	M5a	46,XY[20]	ASXL1 Gly658Ter, NRAS Gly13Arg, RUNX1 Arg201Gln, SRSF2_MFSD Arg94dup, STAG2 Thr918SerfsTer11, TET2 Gln232Ter, TET2 Met1701Ile
AML12	PB	Diagnosis	74	Female	AML	M4	46,XX,t(3;21)(q26.2;q22)[20]	N/A
AML13	PB	Diagnosis	74	Male	AML with myelodysplasia related changes		45,XY,-7[6]/45,XY,-7,der(15)t(7;15)(p12;p11.2)[10]/46,XY[5]	N/A
AML14	PB	Diagnosis	52	Male	AML		45,XY,-7[3]/46,sl,+r(7)(p11q21)[11] /46,sdl1,der(5)t(1;5)(q31;p14)[5]/46,XY[1]	ASXL1, DNMT3a, NOTCH, NRAS
AML15	PB	Diagnosis	51	Male	AML		46,XY,add(1)(p11),del(5)(q15q33),del(7)(q22q36),der(11)t(1;11)(p31;p12-14)[20] , Loss of 5q31 and 7q31	FLT3 ITD, BCOR, NOTCH1
AML16	PB	Diagnosis	85	Male	AML with inv(16)	M4Eo	45,X,-Y,inv(16)(p13.1q22)[10]	N/A
AML17	PB	Diagnosis	74	Female	AML		46,XX[20]	
AML18	PB	Diagnosis	74	Female	AML		46,XX[20]	
AML19	PB	Diagnosis	77	Female	AML with NPM1 mutation		46,XX[20]	NPM1
AML20	PB	Relapse					49~53,XY,+3,+8,+10,+12,+14,+15,+19[cp8]/46,XY[5]	N/A
AML21	PB	Diagnosis	86	Female	AML		46,XX,del(5)(q13q33),+12,der(12;17)(q10;q10)[3]	N/A
AML22	PB	Diagnosis	83	Female	t-AML		46,XX,t(5;15)(p15;q15)[16]/46,XX[4]	N/A
AML23	PB	Diagnosis	84	Female	AML with myelodysplasia related changes		46,XX,del(5)(q13q33),add(7)(p11.2),+8,t(11;12)(q11;p12), -16,-17,?add(17)(q25),add(20)(q11.2),+mar[cp10]	N/A
AML24	PB	Diagnosis	81	Female	AML with NPM1 mutation		46,XX[11]	NPM1, FLT3-ITD
AML25	BM	Refractory					45,X,-Y,t(11;19)(q23;p13.1)[20]	
AML28	PB	Diagnosis	26	Female	AML with monocytic differentiation		46,XX [20]	FLT3-ITD
AML26	BM	Diagnosis	61	Male	Acute Monocytic Leukemia		46,XY[20]	n/a
AML27	BM	Relapse	61	Male	Acute Monocytic Leukemia		46,XY[20]	n/a

PB is peripheral blood; N/A is not available.

Supplemental Table 2 (see excel file): Complete list of SIRT3 interactors identified by BioID and corresponding cellular localization, function, and comparison to published data. Tab 1: SIRT3 BioID Result: peptide counts of SIRT3 interactors compared to negative control with a significant SAINT score. Tab 2: SIRT3 and ClpP/NLN comparison. Data lists all SIRT3 interactors and indicated common interactors with ClpP or NLN identified in previous studies (Ishizawa et al., 2019 and Mirali et al., 2020). An interactor is a protein identified as a SIRT3 interactor that does not interact with ClpP and NLN. Background indicates that the prey protein interacts with ClpP, NLN, and SIRT3. A SIRT3 unique interactor, interacts only with SIRT3. Tab 3 SIRT3 interactor detail: lists all SIRT3 interactors, indicates cellular localization as indicated by the Human MitoCarta 3.0 database, previously reported de-acetylation by SIRT3 (Rardin et al. 2013) or interaction (Yang et al. 2016) and the protein function. BFDR is Bayesian False Discovery Rate; TechRep is technical replicate; #N/A is not available; Y is yes; MIM is mitochondrial inner membrane; SAINT is Significance Analysis of interactome.

Supplemental Table 3: Genes comprising the SIRT3 LSC and SIRT3 AML blasts gene signatures.

SIRT3 LSC	SIRT3 AML Blast
TMEM165	TOP3A
THNSL1	TARS2
TFAM	PNPLA8
SDHB	NT5DC3
PTCD3	NMNAT3
NFU1	GCDH
NDUFS6	FECH
NDUFS1	DLD
NDUFAF1	ALAS1
NDUFA6	
MRRF	
MRPS9	
MRPS7	
MRPS5	
MRPS30	
MRPS25	

MRPL50	
MRPL45	
MRPL43	
MRPL23	
MRPL15	
MRPL10	
LYRM7	
LYRM2	
HADHA	
GRPEL1	
GLRX5	
GADD45GIP1	
FASTKD5	
DNAJC28	
DHX30	
DDX28	
CRAT	
COX6C	
COX5B	
COX5A	
COQ5	
BCKDHA	
ALDH9A1	
ALDH1B1	
AARS2	
PRDX3	
NDUFAB1	
ECH1	
DARS2	

References:

1 Warner, J. K. *et al.* Direct evidence for cooperating genetic events in the leukemic transformation of normal human hematopoietic cells. *Leukemia* **19**, 1794-1805, doi:10.1038/sj.leu.2403917 (2005).

2 Coyaud, E. *et al.* BioID-based Identification of Skp Cullin F-box (SCF)β-TrCP1/2 E3 Ligase Substrates. *Mol Cell Proteomics* **14**, 1781-1795, doi:10.1074/mcp.M114.045658 (2015).

3 Hänzelmann, S., Castelo, R. & Guinney, J. GSVA: gene set variation analysis for microarray and RNA-Seq data. *BMC Bioinformatics* **14**, 7, doi:10.1186/1471-2105-14-7 (2013).

4 Yang, W. *et al.* Mitochondrial Sirtuin Network Reveals Dynamic SIRT3-Dependent Deacetylation in Response to Membrane Depolarization. *Cell* **167**, 985-1000.e1021, doi:10.1016/j.cell.2016.10.016 (2016).

5 Zeng, A. G. X. *et al.* A cellular hierarchy framework for understanding heterogeneity and predicting drug response in acute myeloid leukemia. *Nat Med* **28**, 1212-1223, doi:10.1038/s41591-022-01819-x (2022).

6 Christopher, M. J. *et al.* Immune Escape of Relapsed AML Cells after Allogeneic Transplantation. *New England Journal of Medicine* **379**, 2330-2341, doi:10.1056/NEJMoa1808777 (2018).

7 Li, S. *et al.* Distinct evolution and dynamics of epigenetic and genetic heterogeneity in acute myeloid leukemia. *Nat Med* **22**, 792-799, doi:10.1038/nm.4125 (2016).

8 Shlush, L. I. *et al.* Tracing the origins of relapse in acute myeloid leukaemia to stem cells. *Nature* **547**, 104-108, doi:10.1038/nature22993 (2017).

9 Cocciardi, S. *et al.* Clonal evolution patterns in acute myeloid leukemia with NPM1 mutation. *Nature Communications* **10**, 2031, doi:10.1038/s41467-019-09745-2 (2019).

10 Genomic and Epigenomic Landscapes of Adult De Novo Acute Myeloid Leukemia. *New England Journal of Medicine* **368**, 2059-2074, doi:10.1056/NEJMoa1301689 (2013).

11 Tyner, J. W. *et al.* Functional genomic landscape of acute myeloid leukaemia. *Nature* **562**, 526-531, doi:10.1038/s41586-018-0623-z (2018).

12 Marquis, M. *et al.* High expression of HMGA2 independently predicts poor clinical outcomes in acute myeloid leukemia. *Blood Cancer J* **8**, 68-68, doi:10.1038/s41408-018-0103-6 (2018).

13 Jones, C. L. *et al.* Nicotinamide Metabolism Mediates Resistance to Venetoclax in Relapsed Acute Myeloid Leukemia Stem Cells. *Cell stem cell*, doi:https://doi.org/10.1016/j.stem.2020.07.021 (2020).

14 Stevens, B. M. *et al.* Fatty acid metabolism underlies venetoclax resistance in acute myeloid leukemia stem cells. *Nature Cancer* **1**, 1176-1187, doi:10.1038/s43018-020-00126-z (2020).

15 Dobin, A. *et al.* STAR: ultrafast universal RNA-seq aligner. *Bioinformatics* **29**, 15-21, doi:10.1093/bioinformatics/bts635 (2013).

16 Frankish, A. *et al.* GENCODE reference annotation for the human and mouse genomes. *Nucleic Acids Res* **47**, D766-d773, doi:10.1093/nar/gky955 (2019).

17 Liao, Y., Smyth, G. K. & Shi, W. featureCounts: an efficient general purpose program for assigning sequence reads to genomic features. *Bioinformatics* **30**, 923-930, doi:10.1093/bioinformatics/btt656 (2014).

18 Love, M. I., Huber, W. & Anders, S. Moderated estimation of fold change and dispersion for RNA-seq data with DESeq2. *Genome Biology* **15**, 550, doi:10.1186/s13059-014-0550-8 (2014).

19 Subramanian, A. *et al.* Gene set enrichment analysis: a knowledge-based approach for interpreting genome-wide expression profiles. *Proc Natl Acad Sci U S A* **102**, 15545-15550, doi:10.1073/pnas.0506580102 (2005).
20 Korotkevich, G. *et al.* Fast gene set enrichment analysis. *bioRxiv*, 060012, doi:10.1101/060012 (2021).
21 Merico, D., Isserlin, R., Stueker, O., Emili, A. & Bader, G. D. Enrichment Map: A Network-Based Method for Gene-Set Enrichment Visualization and Interpretation. *PLOS ONE* **5**, e13984, doi:10.1371/journal.pone.0013984 (2010).
22 Ritchie, M. E. *et al.* limma powers differential expression analyses for RNA-sequencing and microarray studies. *Nucleic Acids Res* **43**, e47, doi:10.1093/nar/gkv007 (2015).
23 Benjamini, Y. & Hochberg, Y. Controlling the False Discovery Rate: A Practical and Powerful Approach to Multiple Testing. *Journal of the Royal Statistical Society: Series B (Methodological)* **57**, 289-300, doi:https://doi.org/10.1111/j.2517-6161.1995.tb02031.x (1995).

Supplemental Figure 1

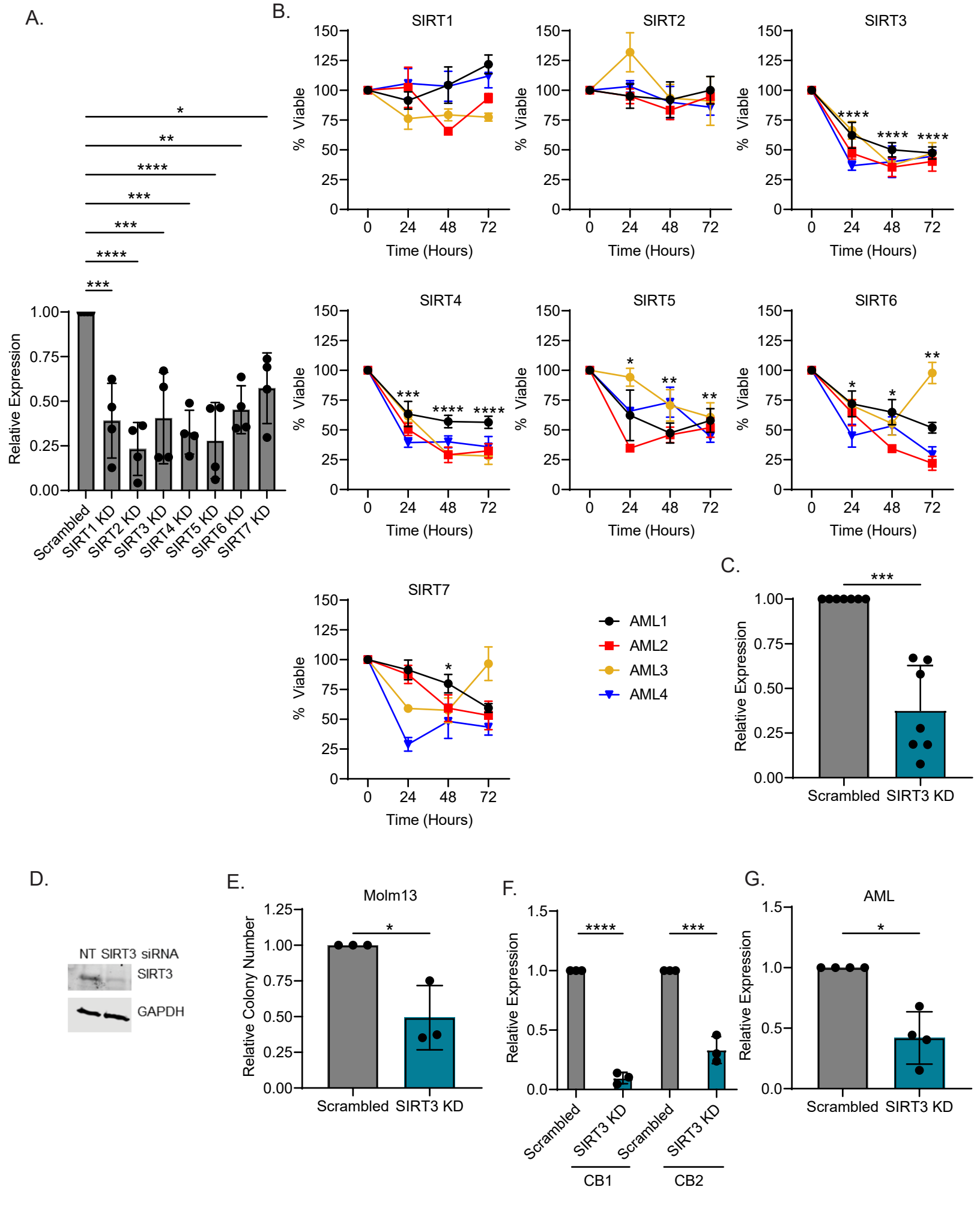

Supplemental Figure 1 Continued

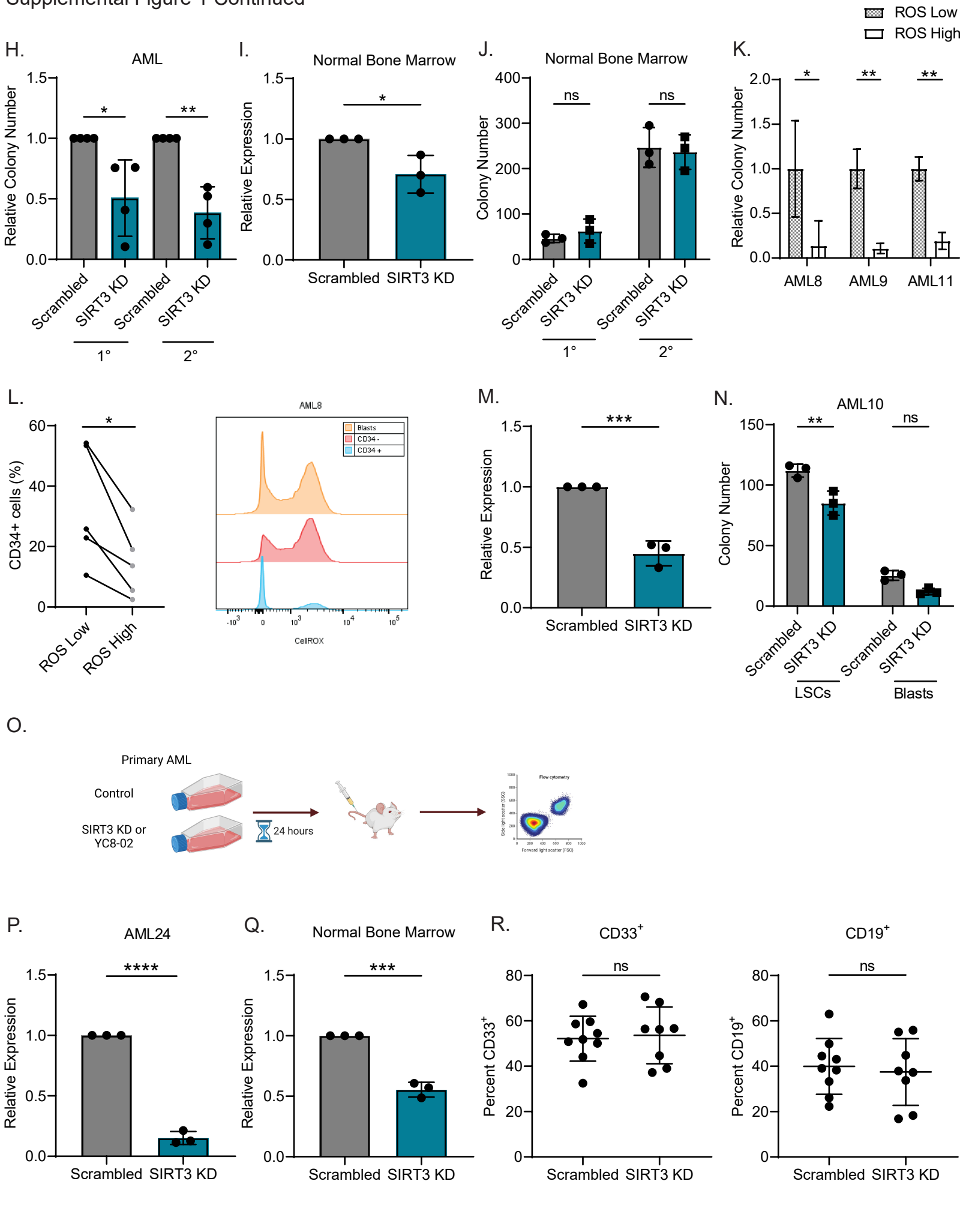

Supplemental Figure Legends:

Supplemental Figure 1: SIRT3 knockdown targets AML but not HSPCs.

(A) mRNA levels of SIRT1-7 in 4 primary AML specimens (AML1-4) 24 hours post scrambled or sirtuin targeting siRNA transfection. Statistical significance was determined by two-way ANOVA analysis. Each dot represents a primary AML specimen. (B) Viability of four primary AML specimens upon SIRT1-7 knockdown at 24-, 48-, and 72-hours post siRNA transfection. Viability is relative to control scrambled siRNA transfected cells. Statistical significance was determined by two-way ANOVA analysis. (C) SIRT3 mRNA 24 hours post scrambled or SIRT3 targeting siRNA transfection in seven primary AML specimens (AML1-5, 14 and 15). Statistical significance was determined using a paired t-test. Each dot represents a primary AML specimen. (D) Representative western blot of SIRT3 and GAPDH 48 hours scrambled control or SIRT3 targeting siRNA transfection in Molm13 cells. (E) Relative colony forming potential of Molm13 cells post scrambled or SIRT3 targeting siRNA transfection. The experiment was repeated three times. Each dot represents a biological replicate. Statistical significance was determined using an unpaired t-test. (F) mRNA expression of SIRT3 relative to GAPDH in CD34 enriched cells from two cord blood samples. Statistical significance was determined by unpaired t-test. (G) mRNA expression of SIRT3 relative to GAPDH in AML samples 9, 10, 11, and 24 post transfection. Statistical significance was determined by unpaired t-test. (H) Colony forming ability of bulk AML samples 9, 10, 11, and 24 post transfection and subsequent secondary replating of colonies. Statistical significance was determined by Ordinary one-way ANOVA analysis. Each dot represents a primary AML specimen. (I) mRNA expression of SIRT3 relative to GAPDH in normal bone marrow post transfection. Statistical significance was determined by unpaired t-test. (J) Colony forming ability of normal bone marrow samples post transfection and subsequent secondary replating of colonies. Statistical significance was determined by Ordinary one-way ANOVA analysis. Each dot represents a technical replicate. (K) Relative colony forming ability of ROS low and ROS high cells enriched from three primary AMLs**.** Statistical significance was determined using unpaired t-tests. (L) Relationship between CD34 expression and ROS levels in primary AML8, AML11, AML12, AML13, AML19, and AML20. Each dot represents a unique primary AML. Statistical significance was determined using paired t-tests. Representative histograms of CellROX staining across bulk, CD34+, and CD34-, cohorts of AML8. (M) mRNA expression of SIRT3 relative to GAPDH in AML sample 10 post transfection. Statistical significance was determined by two-way ANOVA. (N) Colony forming ability of an AML sample sorted into ROS High and ROS low populations and transfected with siRNA. CFU assay was

performed immediately post transfection. (O) Outline of engraftment assay. To assess the function of LSCs upon transfection or YC8-02 treatment, we treated primary specimens with 10uM of YC8-02 for 24 hours, or transfected cells with siRNA targeting SIRT3 or an unscrambled non-targeting control 24 hours prior to injecting approximately 1million cells via tail vein into mice. Engrafted cells were assessed via flow cytometry. (P) mRNA expression of SIRT3 relative to GAPDH in AML sample 24 used for engraftment, post transfection. Statistical significance was determined by unpaired t-test. (Q) mRNA expression of SIRT3 relative to GAPDH in normal bone marrow used for engraftment, post transfection. Statistical significance was determined by unpaired t-test. (R) Percentage of CD33 and CD19 cells collected from normal human bone marrow engraftment assay using transfected bone marrow samples. Statistical significance was determined using unpaired t-tests. All error bars represent standard deviation. *$p<0.05$, **$p<0.01$, ***$p<0.005$, ****$p<0.001$, ns indicates not significant

Supplemental Figure 2

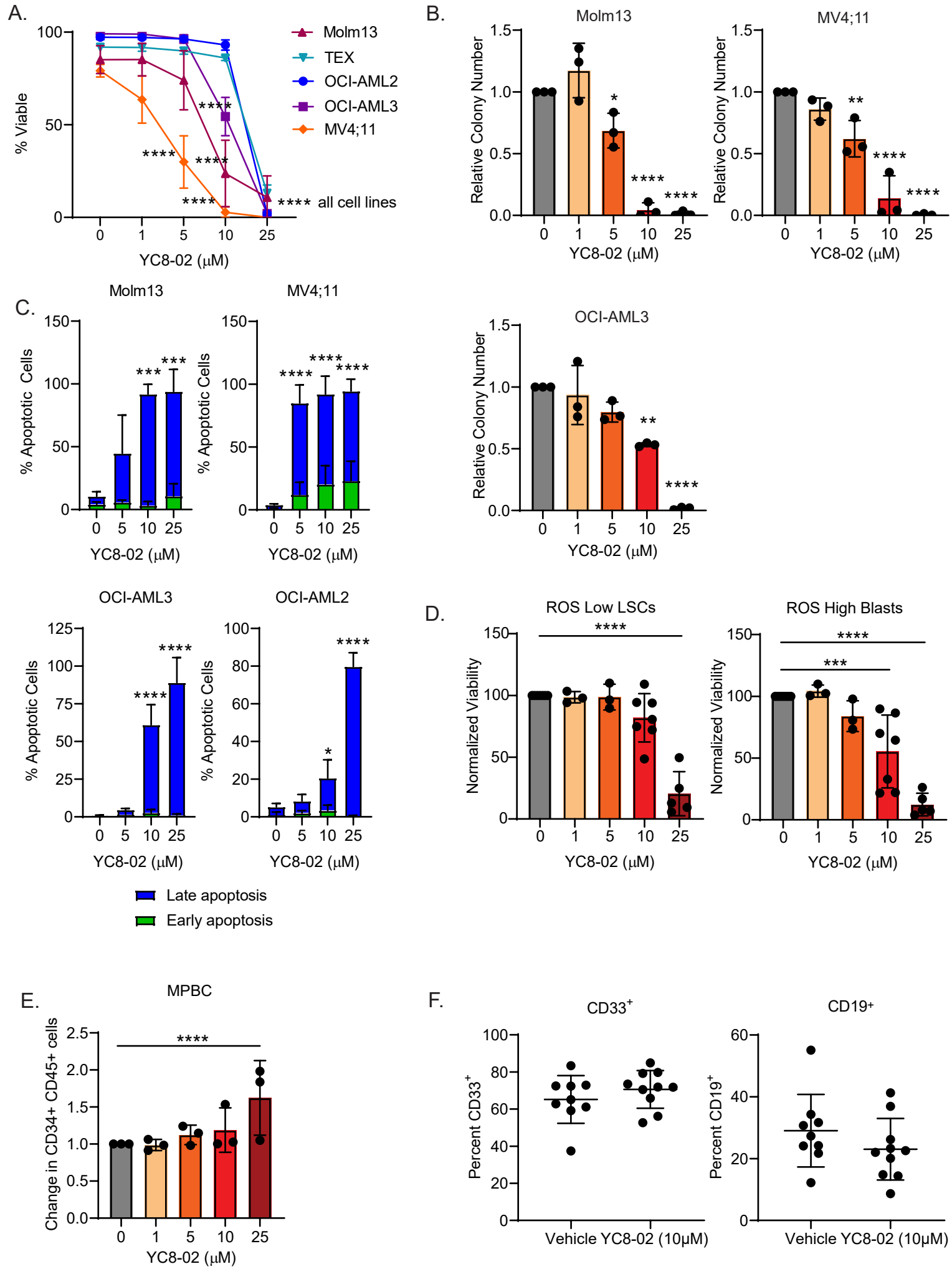

Supplemental Figure 2: SIRT3 inhibition perturbs LSCs function and spares normal HSPCs.

(A) Viability of five AML cell lines treated with YC8-02 for 48 hours. Viability shown is relative to control for each cell lines. Statistical significance was determined using two-way ANOVA. (B) Colony forming ability of three AML cell lines treated with YC8-02 for 24 hours at increasing doses prior to performing the colony forming assay. The experiment was repeated three times and dot represents the mean of three technical replicates. Statistical significance was determined using ordinary one-way ANOVA. (C) Apoptosis in four AML cell lines, measured with Annexin V and DAPI, as a result of 48 hours of YC8-02 treatments. Statistical significance was determined using two-way ANOVA. (D) Viability of ROS low LSCs and ROS high Blasts enriched from ten primary AMLs (AML 4-8 and 10-14) and treated with YC8-02 for 48 hours. Viability is relative to control. Statistical significance was determined using Ordinary one-way ANOVA. (E) CD34+ CD45+ fraction of mobilized peripheral blood cells (MPBCs) collected from three healthy donors following treatment with YC8-02 for 48 hours. Statistical significance was determined using two-way ANOVA. (F) Percentage of CD33 and CD19 cells collected from normal human bone marrow engraftment assay. Statistical significance was determined using unpaired t-tests. All error bars represent standard deviation. *$p<0.05$, **$p<0.01$, ***$p<0.005$, ****$p<0.001$, ns indicates not significant.

Supplementary Figure 3

A.

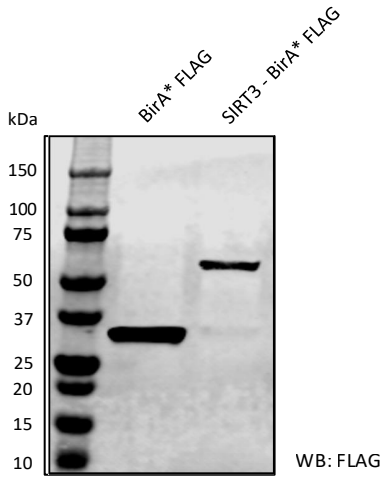

B.

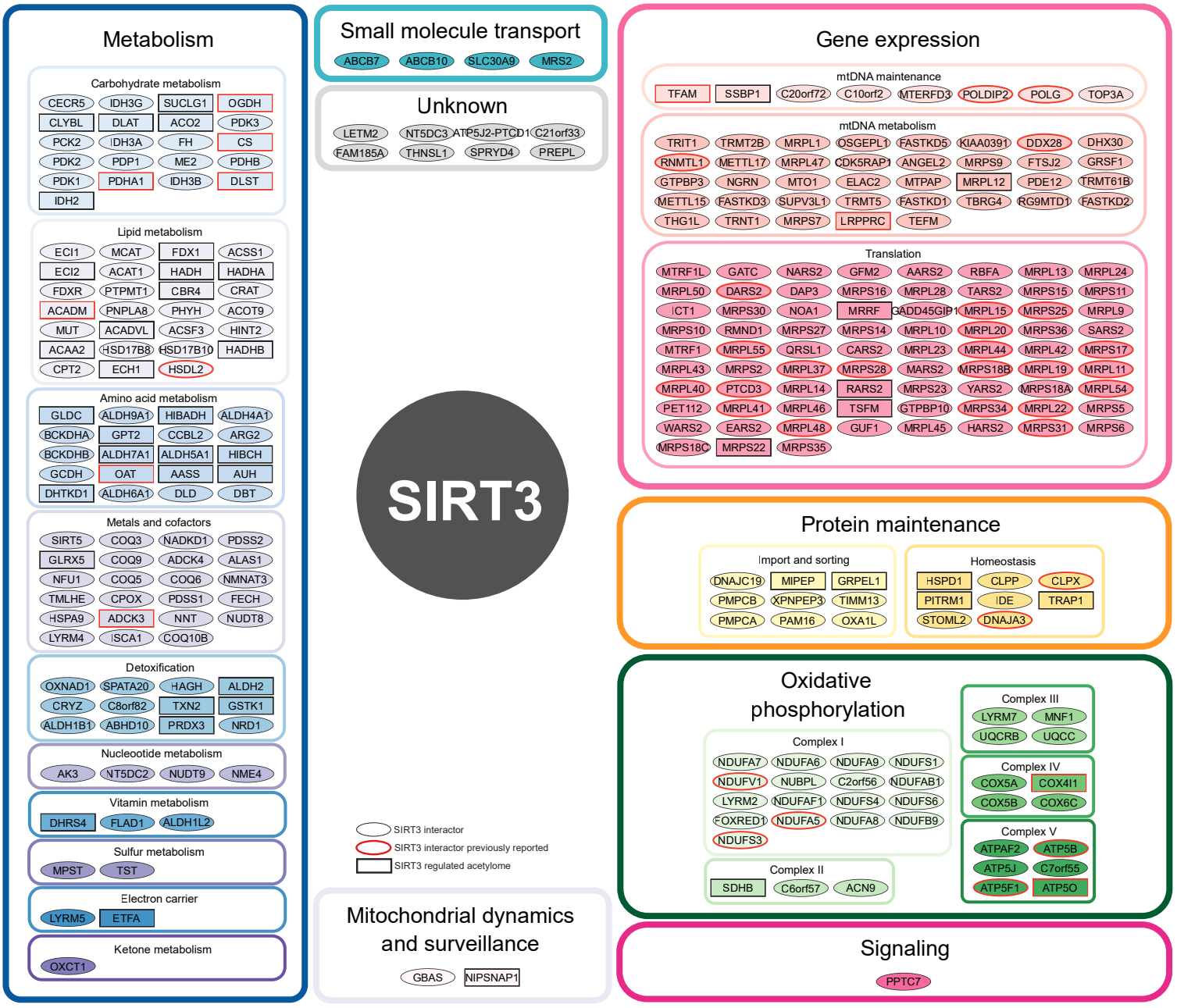

Supplementary Figure 3 Continued

C.

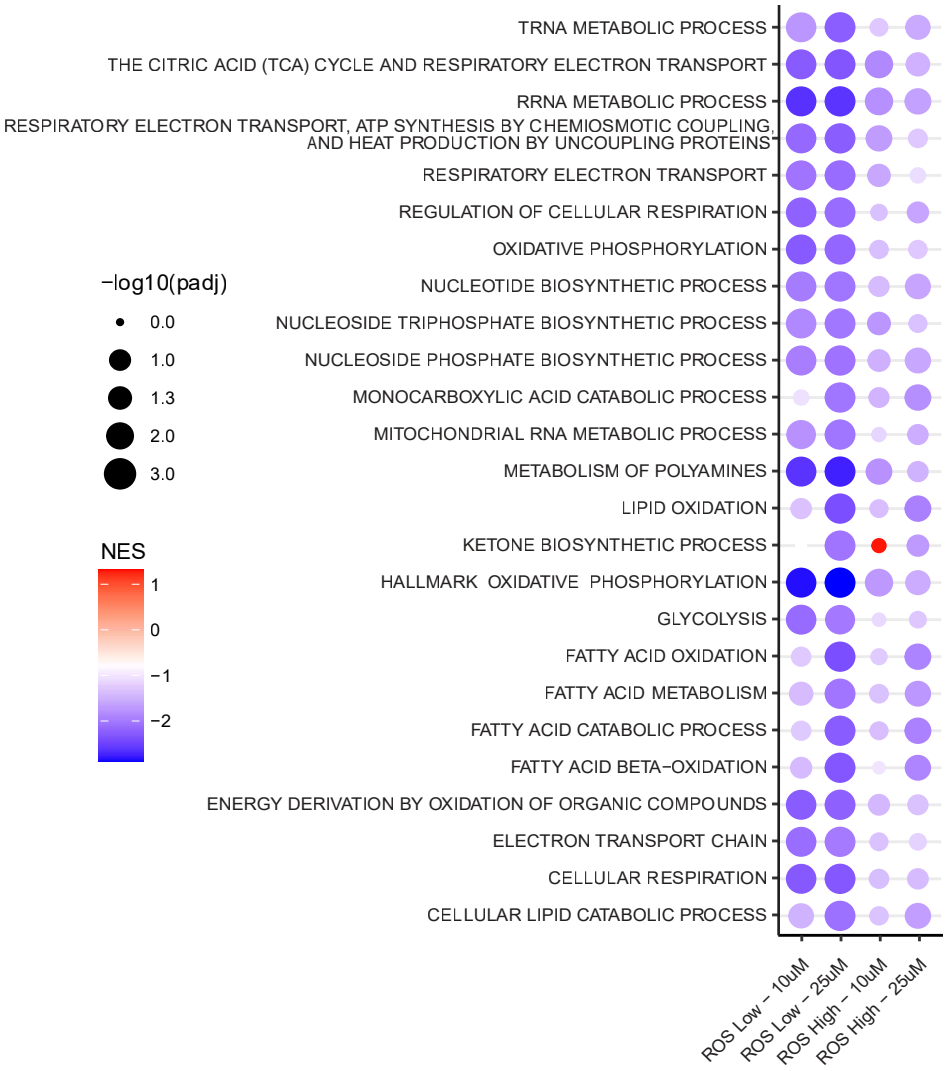

D.

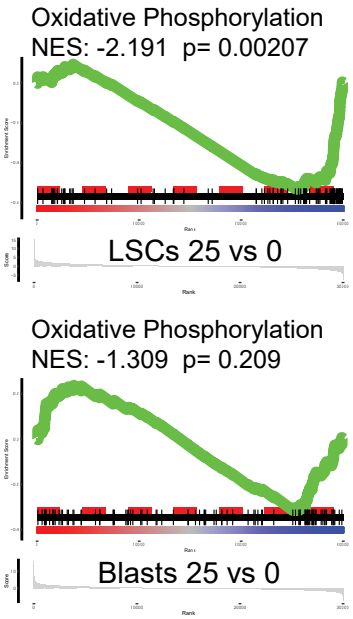

E.

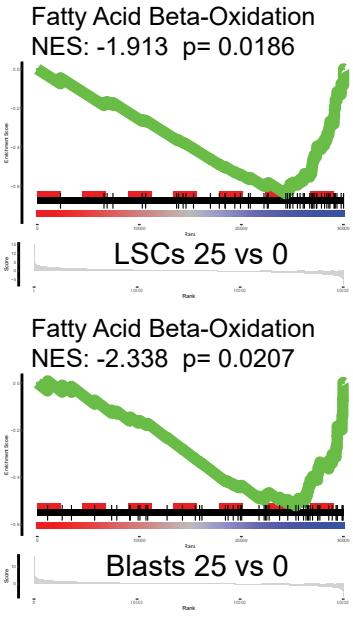

F.

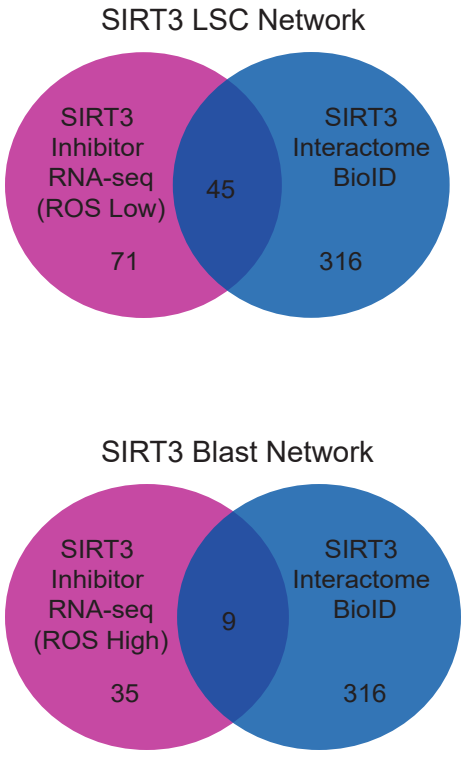

Supplemental Figure 3: SIRT3 regulates mitochondrial energy metabolism in AML.

(A) Expression of BirA*FLAG. BirA*FLAG (control), and SIRT3-BirA*Flag vector. T-Rex cells were lysed and immunoblot was performed with an anti-FLAG antibody 24 hours post induction. (B) Mitochondrial interactions of SIRT3 in T-REx cells found by BioID, grouped based on functional pathways. Interactors outlined in red have been previously described as SIRT3 interactors through IP-MS, and interactors within rectangles have been previously described as de-acetylation targets of SIRT3. (C) Dotplot visualization of top metabolic pathways determined by GSEA. Analysis was performed on RNA-sequencing data from LSCs and AML blasts enriched from three primary AML specimens (AMLs 10, 16 and 17) and treated with 25μM YC8-02 for 4 hours. The color of each dot represents the normalized enrichment score (NES) red (increased) or blue (decreased). The size of each dot represents the significance of the enrichment by –log10 of the adjusted p-value. GSEA of (D) oxidative phosphorylation gene set signature and (E) fatty acid oxidation gene set signature performed on LSCs and AML blasts enriched from three primary AMLs (AMLs 10, 16 and 17) treated with 25μM YC8-02. (F) Schematic of derivation of SIRT3 LSC and SIRT3 blast networks. Overlapping genes identified from unique differentially expressed genes in the YC8-02 treated RNA-seq ROS low or ROS high datasets with SIRT3 interactors identified using BioID were used to create the SIRT3-LSC and SIRT3 blast networks, respectively.

Supplemental Figure 4

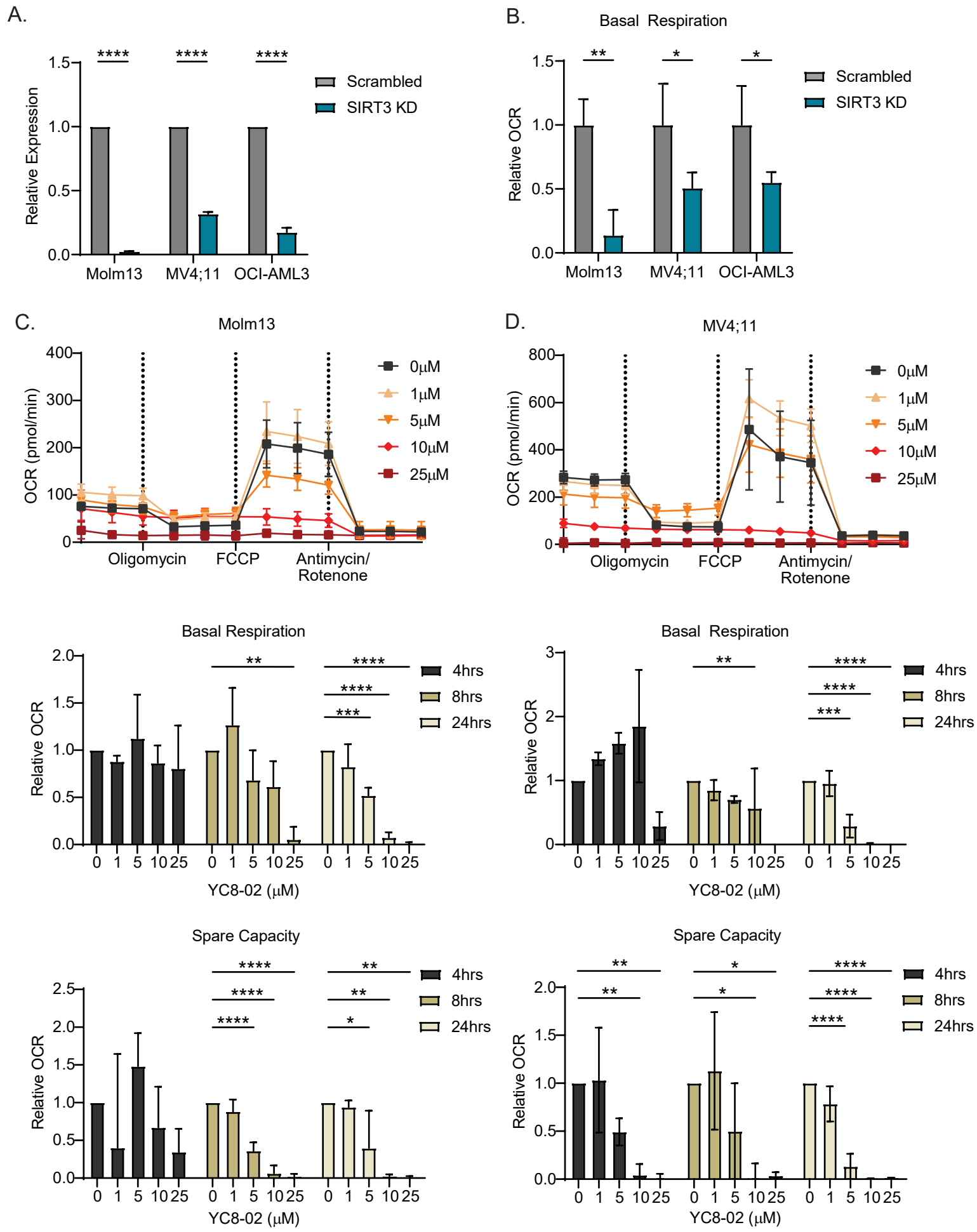

Supplemental Figure 4 Continued

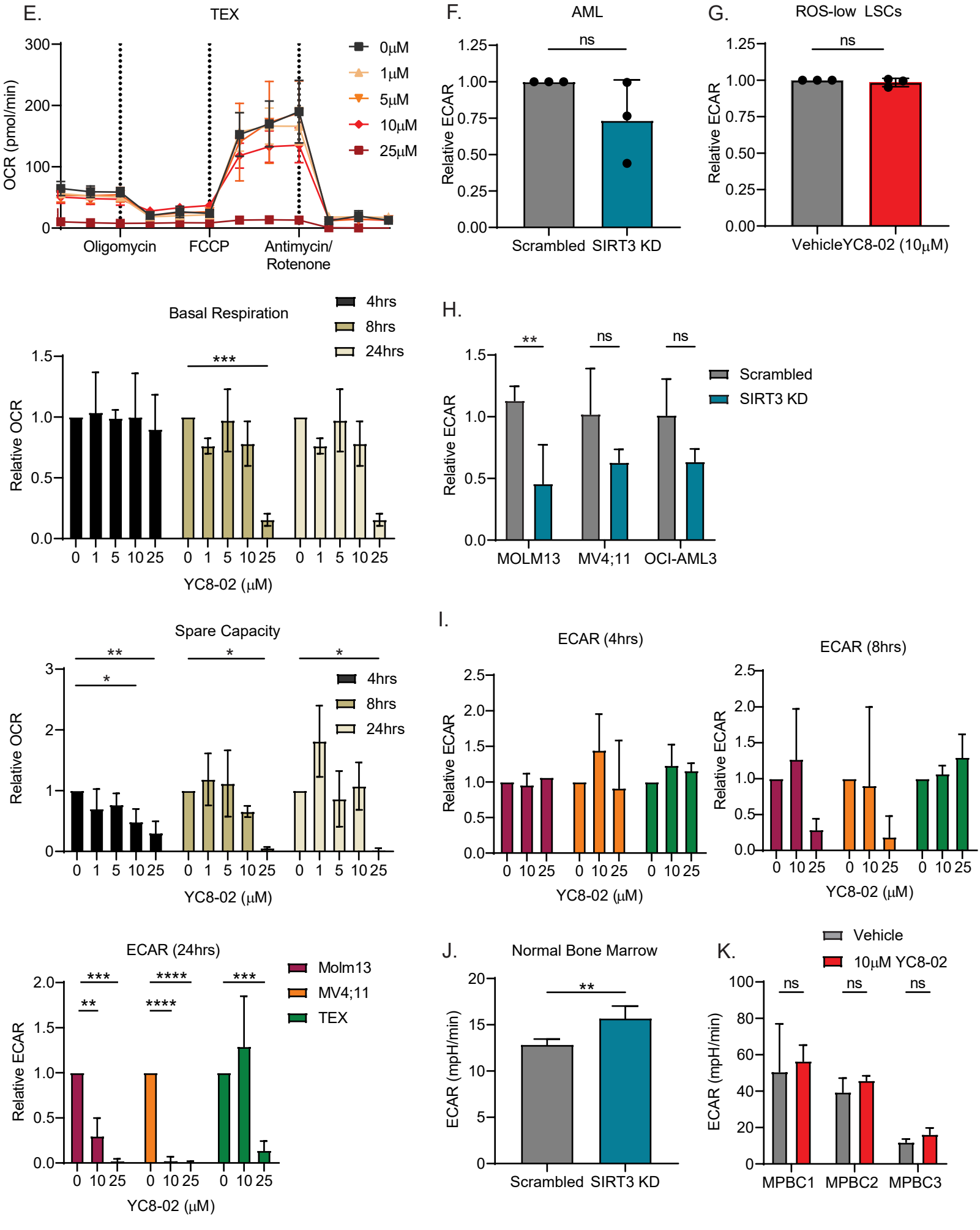

Supplemental Figure 4: SIRT3 regulates oxidative phosphorylation.

(A) mRNA expression of SIRT3 relative to GAPDH in Molm13, MV4;11, and OCI-AML3 cell lines post transfection. Statistical significance was determined by unpaired t-test. (B) Basal respiration of Molm13 cells, MV4;11 and OCI-AML3 cells transfected with siRNA targeting SIRT3 or a non-targeting scrambled siRNA. Measurements taken using n=1, 24 hours post electroporation Statistical significance was determined using two-way ANOVA. Mito stress test profile of (C) Molm13 cells, (D) MV4;11 cells and (E) TEX cells treated with YC8-02 for 8 hours. Parameters of mitochondrial function, basal respiration and spare capacity are reported for each treatment of YC8-02 (0, 1, 5, 10, and 25μM) at three treatment timepoints (4, 8 and 24 hours). Statistical significance was determined using Ordinary one-way ANOVA. (F) ECAR of three bulk primary AML specimens (AMLs 2, 3, and 4) transfected with siRNA targeting SIRT3 or a non-targeting scrambled siRNA. Statistical significance was determined using unpaired t-test. (G) ECAR of LSCs enriched from three primary AML specimens (AMLs 14, 5, and 4) and treated with 10μM of YC8-02. Statistical significance was determined using unpaired t-test. (H) ECAR of Molm13, MV4;11, and OCI-AML3 cells transfected with siRNA targeting SIRT3 or a non-targeting scrambled siRNA. Statistical significance was determined using unpaired t-test. (I) ECAR of Molm13, MV4;11, and TEX cell lines treated with YC8-02 (0, 10, and 25μM) at three treatment timepoints (4, 8 and 24 hours). Statistical significance was determined using two-way ANOVA. (J) ECAR of normal bone marrow transfected with siRNA targeting SIRT3 or a non-targeting scrambled siRNA. Statistical significance was determined using unpaired t-test. (K) ECAR of HSPCs enriched from three mobilized peripheral blood samples and treated with 10μM of YC8-02. Statistical significance was determined using unpaired t-test. Statistical significance was determined using Ordinary one-way ANOVA. All error bars represent standard deviation. *$p<0.05$, **$p<0.01$, ***$p<0.005$, ****$p<0.001$, ns indicates not significant.

Supplementary Figure 5

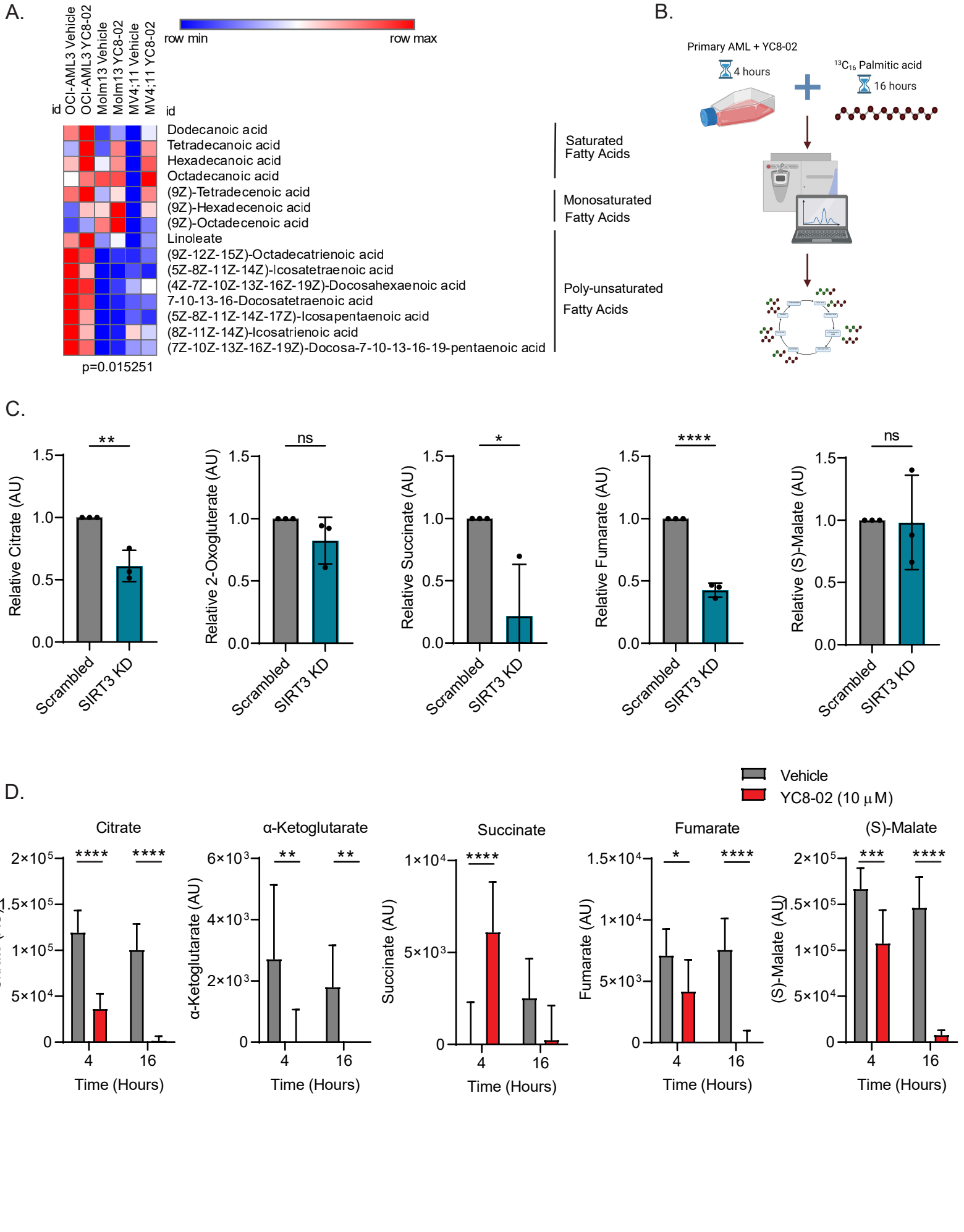

Supplementary Figure 5 Continued

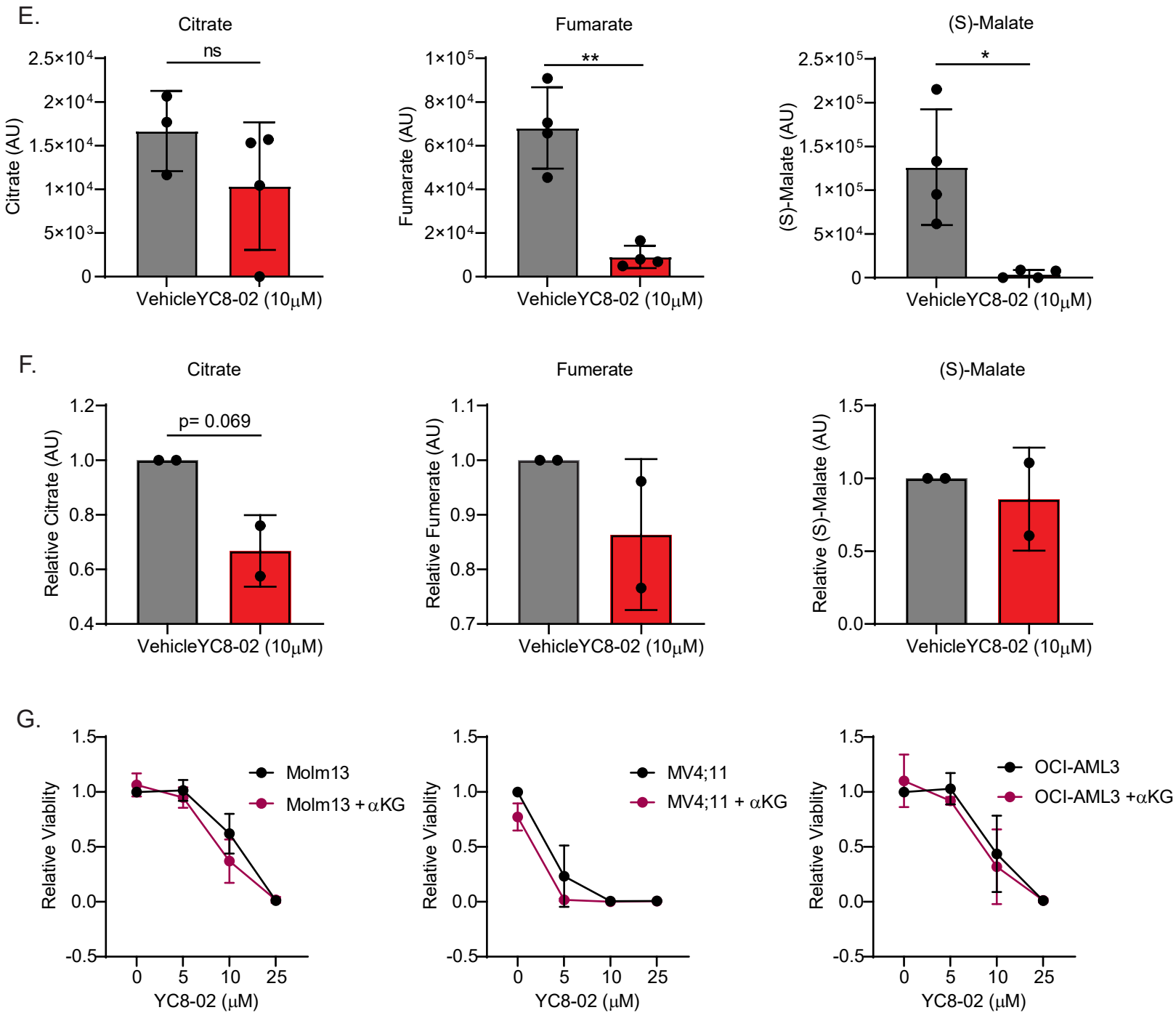

Supplemental Figure 5: SIRT3 inhibition results in fatty acid accumulation in LSCs.

(A) Fatty acids quantities detected by steady state mass-spectrometry lipidomic analysis on three AML cell lines (OCI-AML-3, Molm13, and MV4;11) treated with 10μM YC8-02 for 8 hours. The quantity of each fatty acid detected is represented by color (blue, row minimum, and red, row maximum). Statistical significance was determined using a paired t-test. (B) Experimental design of stable isotope tracing experiments. Briefly, primary AMLs were AMLs treated with 10μM YC8-02 for 4 hours or transfected with siRNA targeting SIRT3 or a non-targeting scrambled siRNA for 24 hours, prior to introduction of U-13C16-palmitate. Cells were incubated an additional 16 hours prior to collection and analysis. Analysis was focused on the change in accumulation of TCA intermediates containing ^{13}C from fatty acid catabolism. (C) Stable isotope tracing analysis of Molm13 cells transfected with siRNA targeting SIRT3 or a non-targeting scrambled siRNA 24 hours prior to introduction of $^{13}C_{16}$-palmitate. Significance was determined using a paired t-test. Stable isotope tracing analysis of (D) Molm13 cells and treated with vehicle or 10μM YC8-02 for 4 hours prior to introduction of 13C1-palmitate. Cells were incubated for an additional 4 or 16 hours before cells were collected and analyzed. Five TCA intermediates were detected from this analysis. Statistical significance was determined using two-way ANOVA. (E) Stable isotope tracing analysis of a bulk AML specimen and treated with vehicle or 10μM YC8-02 for 4 hours prior to introduction of U-13C16-palmitate. Cells were incubated an additional 16 hours before cells were collected and analyzed. Three TCA intermediates were detected from this analysis. Statistical significance was determined using unpaired t-test. (F) Stable isotope tracing analysis of AML blasts enriched from two primary (AMLs 10 and 12) and treated with vehicle or 10μM YC8-02 for 4 hours prior to introduction of U-13C16-palmitate. Cells were incubated an additional 16 hours before cells were collected and analyzed. Three TCA intermediates were detected from this analysis. Statistical significance was determined using unpaired t-test. All error bars represent standard deviation. *$p<0.05$, **$p<0.01$, ***$p<0.005$, ****$p<0.001$, ns indicates not significant. (G) Result of TCA cycle rescue on viability using 3 AML cell lines (Molm13, MV4;11, and OCI-AML3). Cells were treated with dimethyl-2-oxoglutarate (DMKG) at 0 or 2.5mM for 1 hour prior to introduction of increasing doses of YC8-02. Cells were incubated for 48 hours prior to analysis. Statistical significance was determined using an unpaired t-test.

Supplementary Figure 6

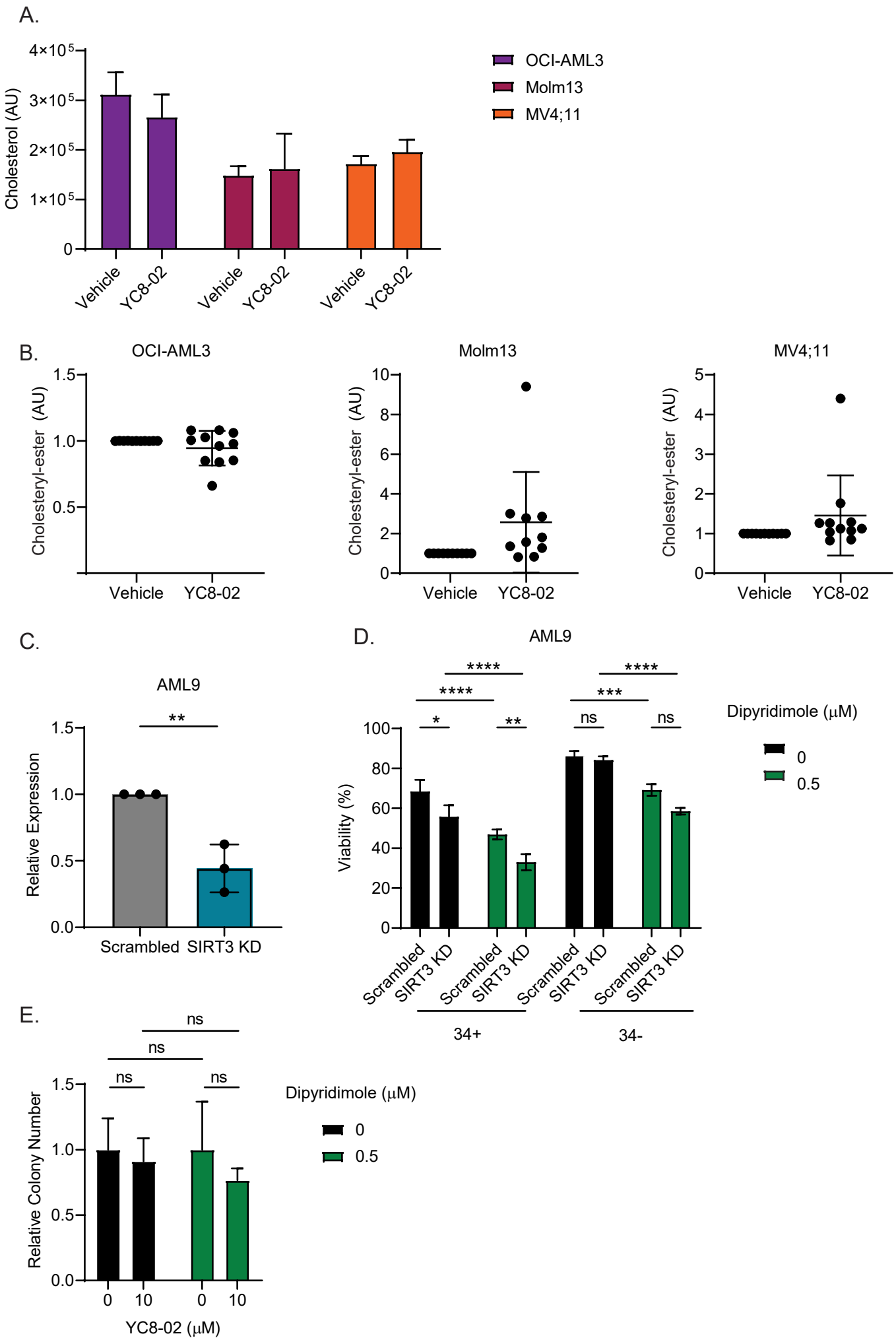

Supplemental Figure 6: Elevated cholesterol metabolism protects LSCs from lipid accumulation

(A) Cholesterol levels detected by steady state mass-spectrometry lipidomic analysis in three AML cell lines (OCI-AML-3, Molm13, and MV4;11) and treated with 10μM YC8-02 for 8 hours. Statistical significance was determined using unpaired t-test. (B) Cholesteryl-ester levels detected by steady state mass-spectrometry lipidomic analysis in three AML cell lines (OCI-AML3, Molm13, and MV4;11) and treated with 10μM YC8-02 for 8 hours. Statistical significance was determined using unpaired t-test. Quantities are normalized to baseline control. (C) mRNA expression of SIRT3 relative to GAPDH in AML sample 9 post transfection. Statistical significance was determined by unpaired t-test. (D) Viability of CD34+ or CD34- cells from bulk AML transfected with siRNA targeting SIRT3 or a non-targeting scrambled siRNA for 24 hours and then treated with 0.5μM dipyridamole. CD34 expression was determined by flow cytometry. Statistical significance was determined using two-way ANOVA. (E) Viability of CB treated with YC8-02 alone or in combination with dipyridamole. Statistical significance was determined using two-way ANOVA. Each normalized Statistical significance was determined using paired t-test. All error bars represent standard deviation. *$p<0.05$, **$p<0.01$, ***$p<0.005$, ****$p<0.001$, ns indicates not significant.